Modeling of Negative Index Metamaterials for "Hide-in-Plain-Sight"

Chiraag Nataraj
Mentor: Dr. Jaret Riddick
Co-Mentor: Dr. Harry Atwater

9/28/2012

Contents

List of Figures

Abstract

The motive of the present research is to investigate the possibility of creating "hide-in-plain-sight" effects using negative index metamaterials (NIMs). The objective is to determine if and how it is possible to use NIMs in order to conceal or disguise an object. In order to investigate these questions, POV-Ray, a raytracing software, is used to model negative index of refraction metamaterials in various configurations. Investigations are conducted based upon varying geometry and gradients of index of refraction to study the effect on an observer's perception of an object enclosed in metamaterial. Results indicate that reflectance and transmittance of a given object are the same whether the index of refraction is positive or negative. Furthermore, using certain combinations of metamaterials and ordinary materials, a variety of optical effects can be achieved. Finally, at certain viewing angles, NIMs are not necessary in order to produce "hide-in-plain-sight" effects - positive index of refraction metamaterials would also work. The present results portend that "hide-in-plain-sight" may not be far off in the future.

1 Introduction

The realization of an autonomous "hide-in-plain-sight" micro-robotic platform of centimeter scale is a goal of Army robotics research. The goal of obscuring a micro-robotic vehicle from a viewer may be approached with the principles of transformation optics which loosely apply Einstein's relativity to electromagnetic theory to conceptualize novel methods to curve the path of light.

In prior work, modeling has been utilized to demonstrate a single-layer, wide-angle, negative-index metamaterial (NIM) through to the blue part of the visible spectrum [1]. The work uses a two-dimensional array of vertically oriented metal-insulator-metal (MIM) coaxial waveguides, arranged in a dense hexagonal configuration, on a flat slab [1]. In addition, metamaterial response has been studied using analytic waveguide modal analysis for single coaxial structures and using finite-difference time-domain (FDTD) simulations for the array of coupled coaxial waveguides. The goal of the present research is to extend the simulations of the flat-slab NIM structure to curved surfaces.

The present research will attempt to produce optical effects using the properties of negative index of refraction materials. Such optical effects include translocation of the object, multiplication of the object (seeing more than one where there is only one), disguising the true size of the object (making it look bigger or smaller than it actually is).

The assumption used in these simulations is that the materials do not absorb any electromagnetic radiation – all the EM radiation is either transmitted or reflected.

2 Background

2.1 Concepts

2.1.1 Permeability of a material

The permeability of a material describes the ability of the material to support the formation of a magnetic field. It is denoted by the symbol μ. The permeability of free space, denoted by μ_0, is $4\pi \times 10^{-7} \frac{\text{newtons}}{\text{amperes}^2}$ [7]. Free space is a vacuum.

2.1.2 Permittivity of a material

The permittivity of a material describes how much resistance is encountered when forming an electric field in that material. It is denoted by the symbol ε. The permittivity of free space, denoted by ε_0, is

$$\varepsilon_0 = \frac{1}{c_0^2 \mu_0} \tag{1}$$

where c_0, which has an exact value of $2.99792458 \times 10^8 \frac{\text{meters}}{\text{second}}$, is the speed of light in a vacuum [7].

2.1.3 Maxwell's Equations in Free Space

Maxwell's Equations in Free Space are given below:

$$\vec{\nabla} \cdot \vec{E} = 0 \tag{2}$$

$$\vec{\nabla} \cdot \vec{B} = 0 \tag{3}$$

$$\vec{\nabla} \times \vec{E} = -\frac{\partial \vec{B}}{\partial t} \tag{4}$$

$$\vec{\nabla} \times \vec{B} = \mu_0 \varepsilon_0 \frac{\partial \vec{E}}{\partial t} \tag{5}$$

[5]. Equation (2) equates the divergence of the electric field with 0. This implies that there is no net charge in free space. Equation (3) equates the divergence of the magnetic field with 0. This implies there is no net current in free space as well. Equation (4) equates the curl of the electric field with the negative time rate of change of the magnetic field (the ∂t symbolizes a partial derivative with respect to time). Equation (5) equates the curl of the magnetic field with the permittivity of free space multiplied by the permeability of free space multiplied by the time rate of change of the electric field. This set of equations governs the passage of any electromagnetic radiation through free space. In addition, these can be used as an approximation for the passage of electromagnetic radiation through air, as the speed of light is almost the same through vacuum and air. If one solves the set of equations above, one obtains the speed of light defined in terms of the permeability and permittivity:

$$c = \frac{1}{\sqrt{\mu_0 \varepsilon_0}} \tag{6}$$

2.1.4 Index of Refraction of a material

Light, however, does not always travel at the same speed. For example, light travels slower in water than in air, and even slower in diamond. The number which quantifies the speed at which light travels through a given medium is called the index of refraction. The index of refraction is the ratio of the speed of light in vacuum to the speed of light in a particular material.

$$n^2 = \varepsilon \mu \tag{7}$$

$$= \frac{c^2}{v^2} \tag{8}$$

[12] where μ, ε, and v are properties of the material for which the index of refraction is sought. μ is the material's permeability, ε is the material's permittivity, and v is the speed of light in the material. From Equation (8), note that the index of refraction can be positive or negative. The commonly accepted formula for the index of refraction, given in Equation (9), implies that the index of refraction can only be positive. Indeed, materials found in nature always have positive indices of refraction. However, Veselago proved [12] that a negative index of refraction is within the realm of physical possibility.

$$n = \frac{c}{v} \tag{9}$$

2.1.5 Snell's Law

Snell's Law is illustrated in Figure 1 and given by Equation (10)

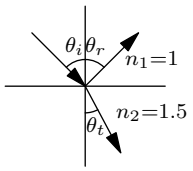

Figure 1: Snell's Law

$$n_1 \sin\theta_i = n_2 \sin\theta_t \tag{10}$$

[5] where n_1 is the index of refraction of the 'outside' material (usually air), n_2 is the index of refraction of the material itself, θ_i is the angle of incidence (the angle with which the light ray hits the material) as measured

from the vertical, and θ_t is the angle with which the transmitted ray continues through the material. This law holds true in negative index of refraction metamaterials as well (as it must). However, the outcome changes slightly. In Figure 2, Snell's Law is illustrated for an interface between air and a negative index of refraction metamaterial. The variables are the same as before. This time, however, the transmitted light

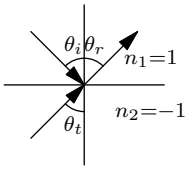

Figure 2: Snell's Law for a Negative Index of Refraction Metamaterial

ray gets refracted to the opposite side - that is, there is a negative angle of refraction. In addition, note that the direction of wave propagation is reversed.

2.1.6 Fresnel Equations

The Fresnel Equations is a group of equations derived from Maxwell's Equations which quantifies how much light is reflected and how much light is transmitted when light passes into a given medium. In order to derive these equations, however, ordinary light must be divided into two different types of polarized light - TE and TM. TE is transverse electric and means that there is no electric field in the plane of incidence. TM is transverse magnetic and means that there is no magnetic field in the plane of incidence [5]. Figures 3a and 3b show these two different cases. Ordinary, unpolarized light is a mixture of these two modes in equal components. Here, $\vec{E}$ is the electric field, $\vec{B}$ is the magnetic field, and $\hat{k}$ is the direction of wave propagation.

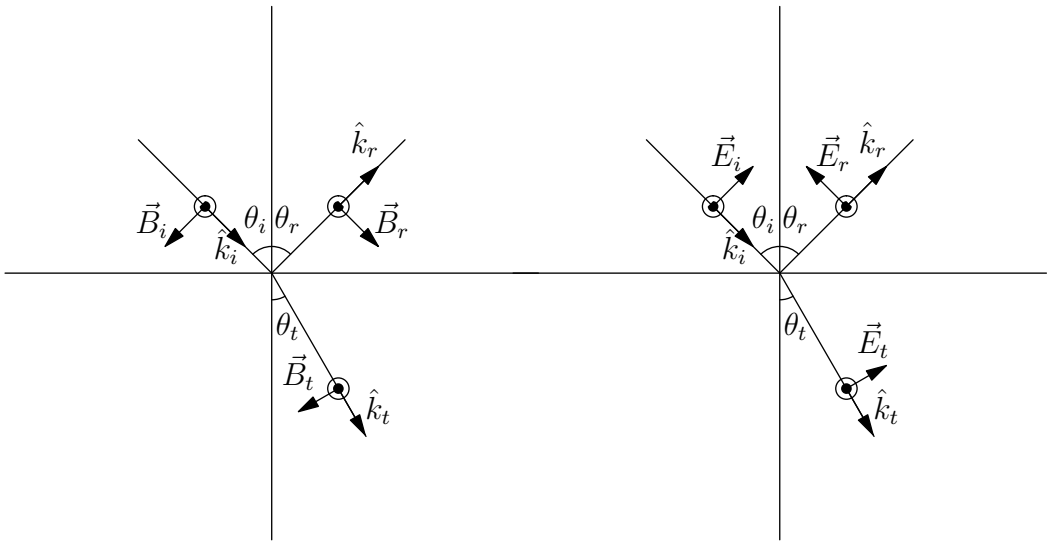

(a) TE-polarized EM waves (b) TM-polarized EM waves

Figure 3: TE and TM polarized electromagnetic radiation

The subscript 'i' means "initial", 'r' means "reflected", and 't' means "transmitted". However, Figures 3a and 3b are for ordinary materials. In negative index of refraction metamaterials, the diagrams change slightly as a result of the reversed direction of wave propagation ("negative velocity") and the reversed refraction angle due to Snell's Law. Figures 4a and 4b are the equivalent figures for negative index of refraction metamaterials. With this modified setup, the question is whether the Fresnel Equations are valid. They are indeed valid and the proof is given in Appendix A.

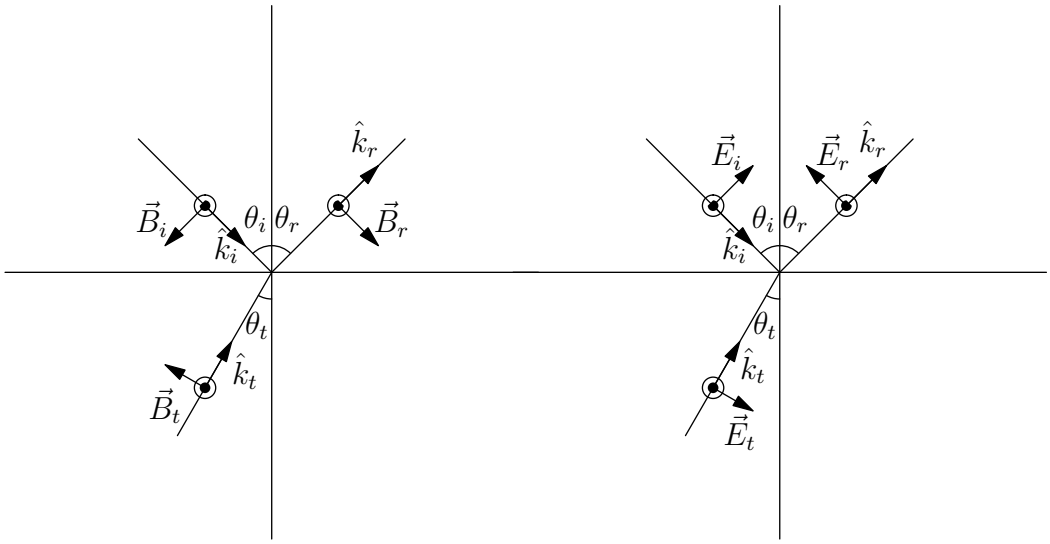

(a) TE-polarized EM waves (b) TM-polarized EM waves

Figure 4: TE and TM polarized electromagnetic radiation for a negative index of refraction metamaterial

2.2 Tools

2.2.1 Ray Tracing

Ray Tracing is a technique used in order to simulate a viewer's perspective of an object. Ray Tracing accomplishes this by tracing rays of light into a scene and recording when the ray hits an object. If the object is translucent, the program will use the Fresnel Equations in order to compute how much of the light is reflected and how much is transmitted based on the index of refraction and angle of incidence. Normally, forward ray tracing – that is, from the light to the eye – is extremely inefficient. Therefore, most ray tracers, by default, do backward ray tracing – that is, from the eye to the light. However, in order to simulate certain effects such as caustics, the projection of rays reflected off of one surface onto another, it is imperative that forward ray tracing be used, as backward ray tracing will not accurately simulate those effects – it a limitation of that technique.

3 Methods

For the purposes of this research, the ray tracing software POV-Ray (http://povray.org) was used. Five different structures were investigated: Cube (Figure 5a), Sphere (Figure 5b), Slab (Figure 5c), Curved Slab (Figure 5d), and Saddle Slab (Figure 5e). Four different material gradient scenarios were investigated of each of those structures: Solid (Figure 6a), Gradient (2 types - Figures 6b and 6c), Embedded Object (Figure 6d), and Surface Gradient (Figure 6e). Several simulations were run of each scenario with each structure.

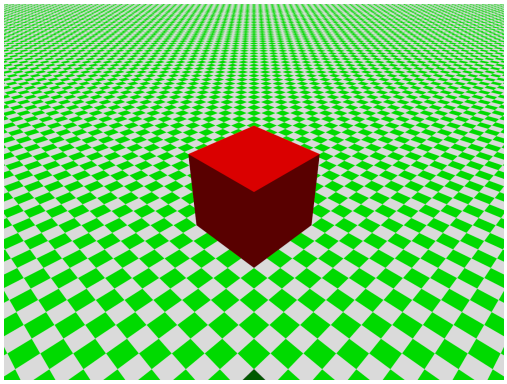

(a) Cube

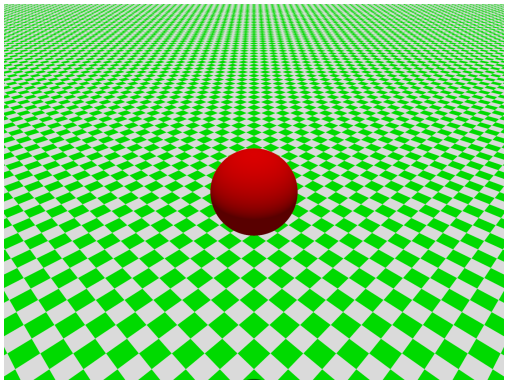

(b) Sphere

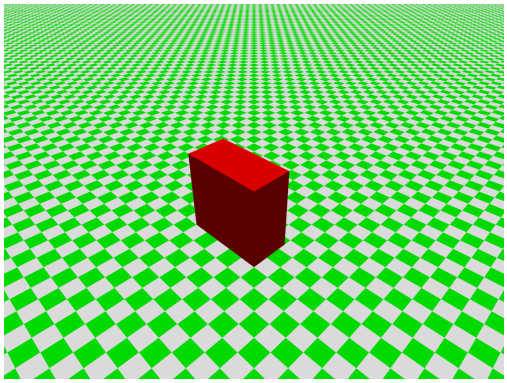

(c) Slab

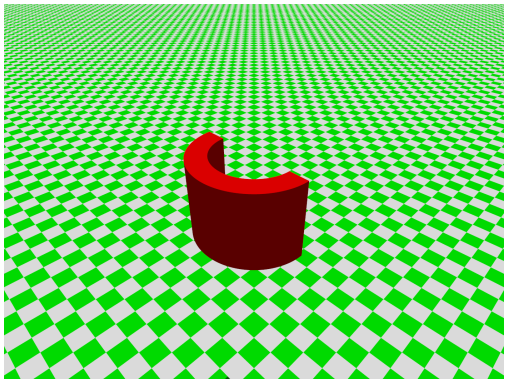

(d) Curved Slab

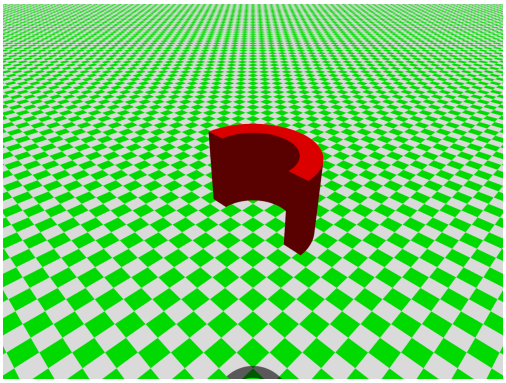

(e) Saddle Slab

Figure 5: Structures

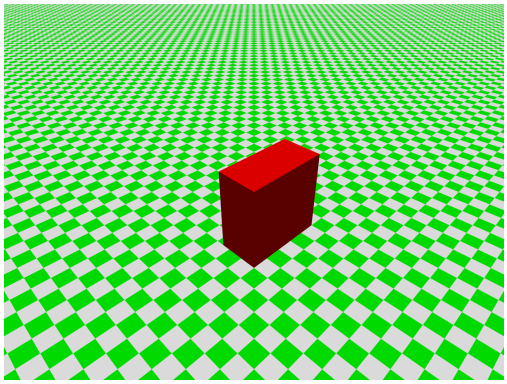

(a) Solid

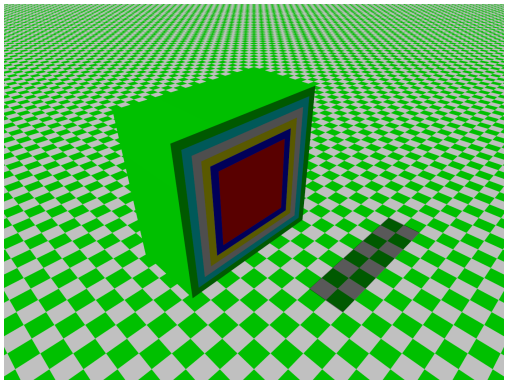

(b) Gradient (the red object in the middle is the object to be hidden)

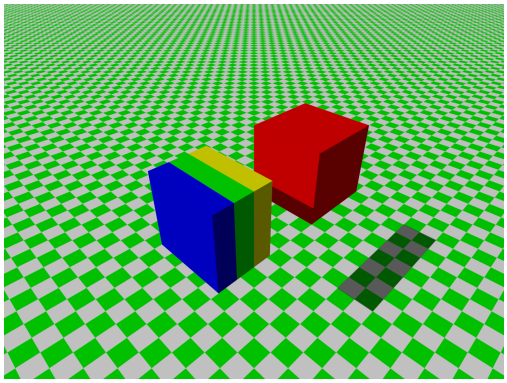

(c) Gradient (the red object is the object to be hidden)

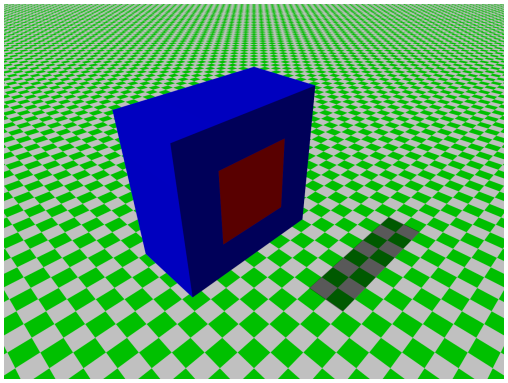

(d) Embedded (the red object in the middle is the object to be hidden)

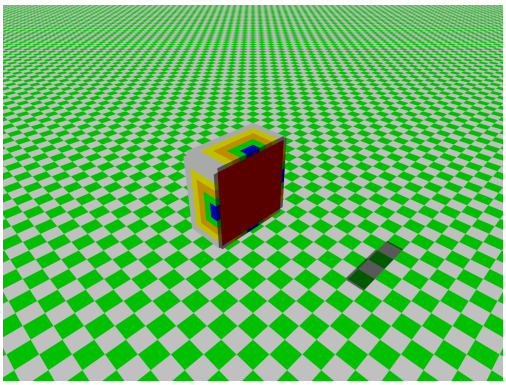

(e) Surface Gradient (the red object in the middle is the object to be hidden)

Figure 6: Scenarios (a cube has been cut open to show the inside)

4 Results

4.1 Solids

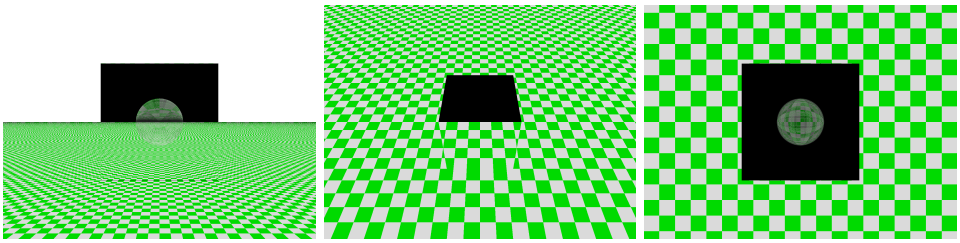

(a) Cube 2 cm x 2 cm x 2 cm. Index of Refraction (IOR): -0.1. View: X axis

(b) Cube 2 cm x 2 cm x 2 cm. IOR: -0.1. View: 45°

(c) Cube 2 cm x 2 cm x 2 cm. IOR: -0.1. View: Z axis

Figure 7: Solids - Cubes

The results shown in Figures 7a and 7c indicate that given a sufficiently low index of refraction (IOR) (-0.1 in this case), a solid cube looks like it contains a spherical object, but only from certain angles. From others, as in Figure 7b, it looks like it contains nothing at all. Note that the cube is *not* transparent - it is merely reflecting from the floor (checker pattern) and sky (black). In Figures 8a-f, a solid sphere appears to contain a sphere (or multiple spheres) inside it. This effect occurs for more than one (negative) index of refraction - in this case, -0.5 as well as -1.5. Figures 9a and 9b show that while the slab with an IOR of $\frac{1}{\sqrt{2}}$ appears beveled, the slab with an IOR of $-\frac{1}{\sqrt{2}}$ is virtually invisible. Figures 10a and 10b show that the curved slab with the negative index of refraction disturbs the background less than the curved slab with the positive index of refraction. The same can be said of Figures 11a and 11b.

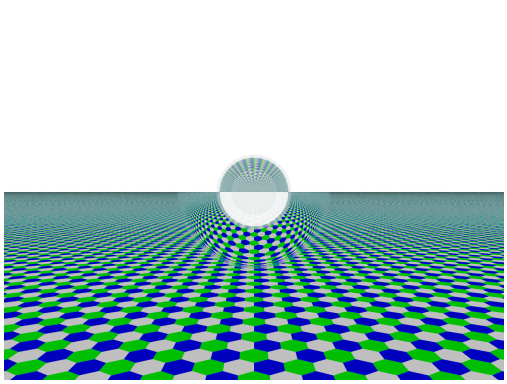

(a) Sphere with radius 1 cm. IOR: -0.5. View: X axis

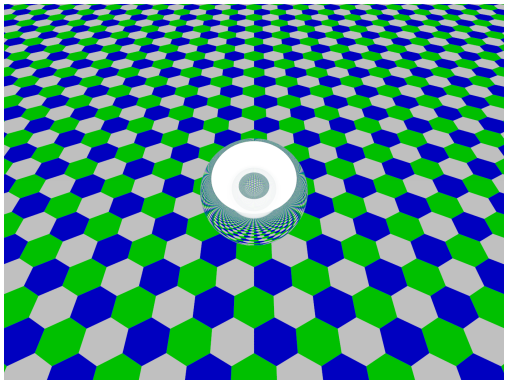

(b) Sphere with radius 1 cm. IOR: -0.5. View: 45°

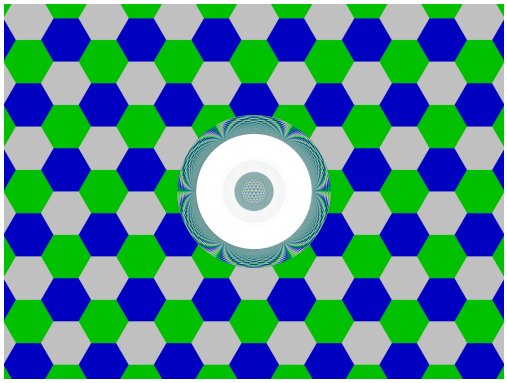

(c) Sphere with radius 1 cm. IOR: -0.5. View: Z axis

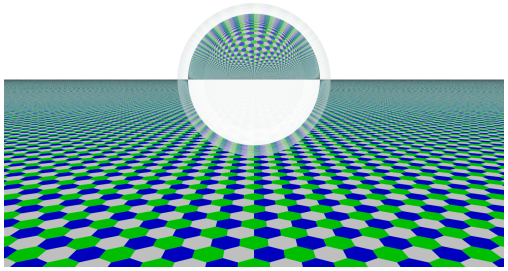

(d) Sphere with radius 1 cm. IOR: -1.5. View: X axis

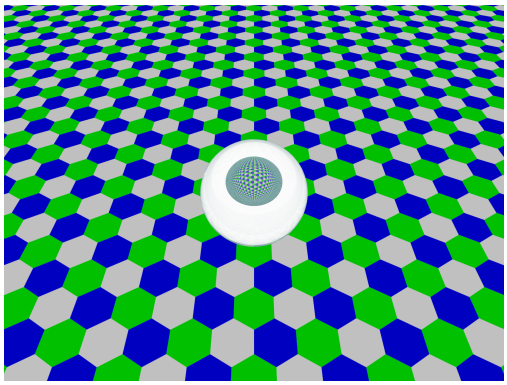

(e) Sphere with radius 1 cm. IOR: -1.5. View: 45°

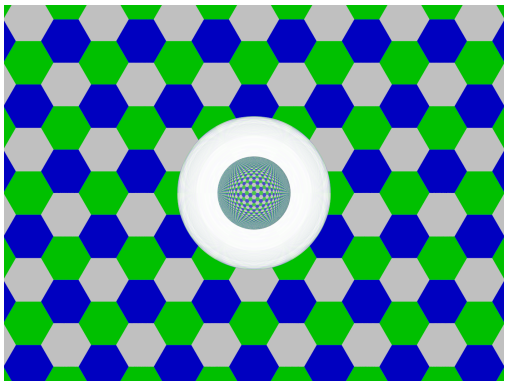

(f) Sphere with radius 1 cm. IOR: -1.5. View: Z axis

Figure 8: Solids - Spheres

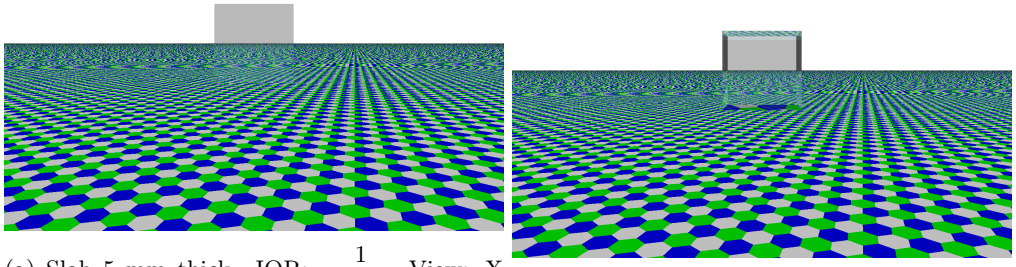

(a) Slab 5 mm thick. IOR: $-\frac{1}{\sqrt{2}}$. View: X axis

(b) Slab 5 mm thick. IOR: $\frac{1}{\sqrt{2}}$. View: X axis

Figure 9: Solids - Slabs

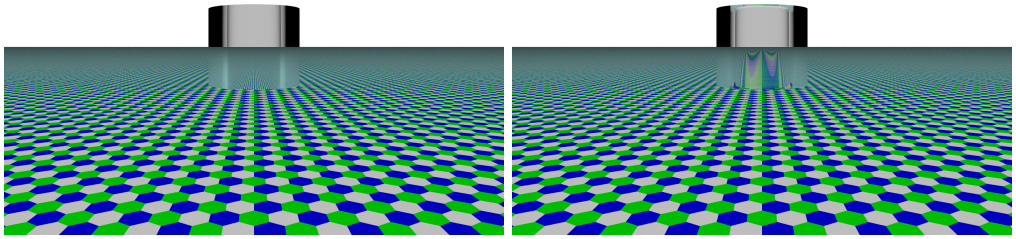

(a) Curved Slab 300 nm thick. IOR: $-\frac{1}{\sqrt{2}}$. View: X axis

(b) Curved Slab 300 nm thick. IOR: $\frac{1}{\sqrt{2}}$. View: X axis

Figure 10: Solids - Curved Slabs

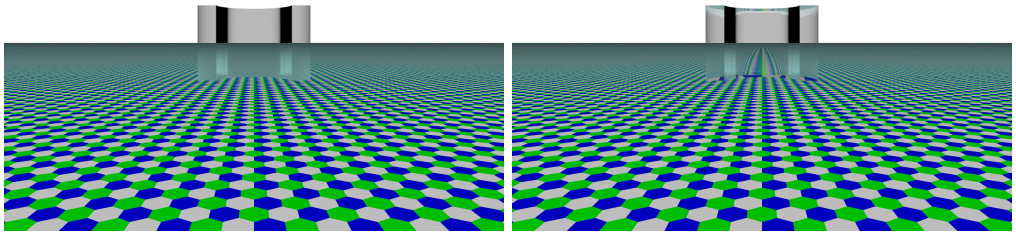

(a) Saddle Slab 5 mm thick. IOR: $-\frac{1}{\sqrt{2}}$. View: X axis

(b) Saddle Slab 5 mm thick. IOR: $\frac{1}{\sqrt{2}}$. View: X axis

Figure 11: Solids - Saddle Slabs

4.2 Gradients

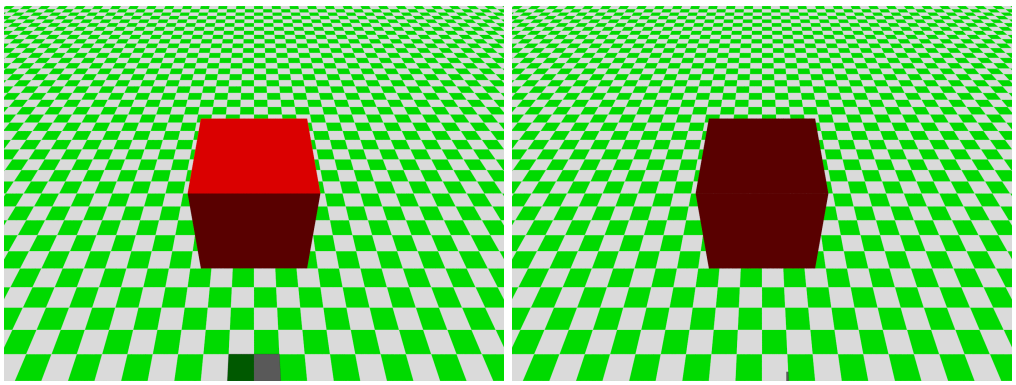

(a) Comparison cube (2 cm x 2 cm x 2 cm). View: 45°

(b) Cube 300 nm thick. Gradient in IOR: -2.3 to -1, working outward. View: 45°

Figure 12: Gradients - Cubes

In Figure 12b, one can see how the apparent color of the cube changes with respect to Figure 12a. In Figure

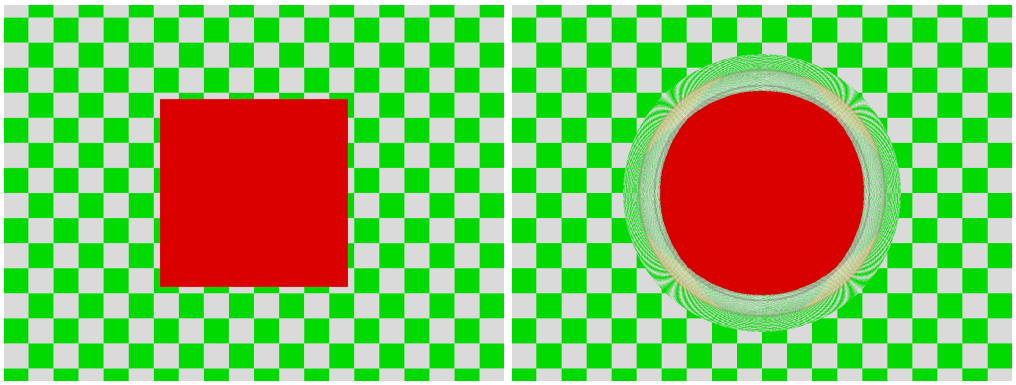

(a) Comparison cube (2 cm x 2 cm x 2 cm). View: Z axis

(b) Sphere. Gradient in IOR: -1.1 to -0.9, working outward. Varies in thickness due to the object being a cube. View: Z axis

Figure 13: Gradients - Spheres

13b, a sphere with a gradient like that of Figure 6b in the IOR managed to disguise the cube seen in Figure 13a. In Figures 14b and 14c, the slab with a gradient in the IOR makes the cube shown in 14a look larger. Even more remarkable is that Figure 14b manages to make the object appear larger without hinting of its presence. By contrast, in Figure 14c, the gradient leaves its mark on the object – note the slight white squares patterned on the cube. In Figures 15b and 15c, the curved slab with a gradient in IOR working outward (as in Figure 6b) can change the number of objects perceived as compared to Figure 15a. In Figures 15d and 15e, the curved slab with a gradient in IOR through the thickness (as in Figure 6c) can change the perceived shape of the object as compared to Figure 15a. In Figures 16b and 16c, the saddle slab with a gradient in IOR through the thickness can change how the object is perceived as compared to Figure 16a – the cube is compressed in the x direction, making it appear as a rectangular prism.

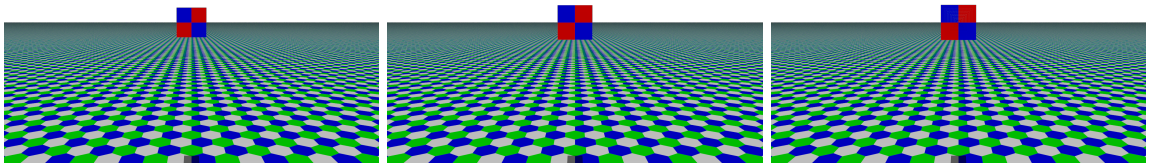

(a) Comparison cube (2 cm x 2 cm x 2 cm). View: X axis

(b) Slab 300 nm thick. Gradient in IOR: -1.1 to -1, working outward. View: X axis

(c) Slab 300 nm thick. Gradient in IOR: -2.3 to -1, working outward. View: X axis

Figure 14: Gradients - Slabs

4.3 Embedded Objects

In Figure 17b, one can see that an object (Figure 17a) can be all but hidden by covering it with a material with an index of refraction of $\frac{1}{\sqrt{2}}$. Notice how a negative index of refraction is not necessarily required for this effect. However, this material only disguises the object for a limited amount of angles - it is perfect at 45°, but imperfect at any angle greater than 50° or less than 40°. However, Figure 17d shows an object (Figure 17c) being hidden by covering it with a material with an index of refraction of -0.001. This material, on the other hand, works at all angles. In Figure 18b, one can see how a cube (Figure 18a) has been made to superficially resemble a sphere by enclosing it in a spherical material of radius $\sqrt{3}$ + 0.00003cm. In Figure 18d, one can see how a sphere (Figure 18c) appears smaller when encased in a spherical material of radius 1.00003 cm. In Figure 19b, one can see how a cube (Figure 19a) appears as a sphere when a slab 5 mm thick with an index of refraction of -0.1 is placed 2 cm in front of it. In addition, the pattern on the object is extremely distorted. In Figure 20b, the object (Figure 20a) has been distorted horizontally by a curved slab 3 mm thick with an index of refraction of $-\frac{1}{\sqrt{2}}$. In Figure 20c, the object (Figure 20a) disappears when placed behind a curved slab with an index of refraction of -0.01 stretched by a factor of 1.5 in the X direction. In Figure 21b, it appears that there is more than one object. This effect is displayed when the object (Figure 21a) is placed behind a saddle slab 300 nm thick with an index of refraction of -2.3.

4.4 Surface Gradients

In Figure 22b, the results show that while the object (Figure 22a) does look a bit larger and does have lines on it, as well as reflecting a lot more light, there is not much difference between the two figures. In Figure 23b, the object (Figure 23a) appears larger when placed behind a slab 300 nm thick with a surface gradient from -1.1 (inside) to -0.9 (outside).

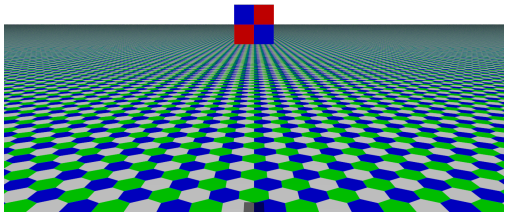

(a) Comparison cube (2 cm x 2 cm x 2 cm). View: X axis

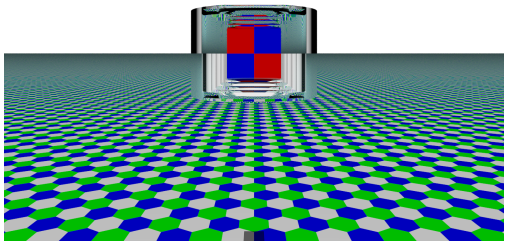

(b) Curved Slab 300 nm thick. Gradient in IOR: -1.1 to -0.9, working outward. View: X axis

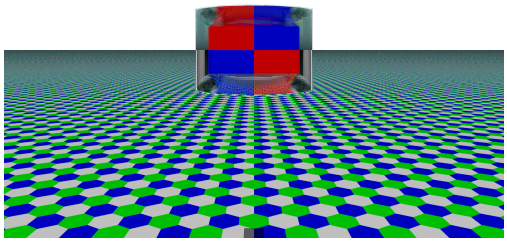

(c) Curved Slab 300 nm thick. Gradient in IOR: -2.3 to -1, working outward. View: X axis

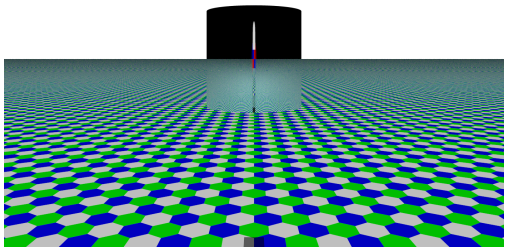

(d) Curved Slab 300 nm thick. Gradient in IOR: 0.1 to 1, through the thickness. View: X axis

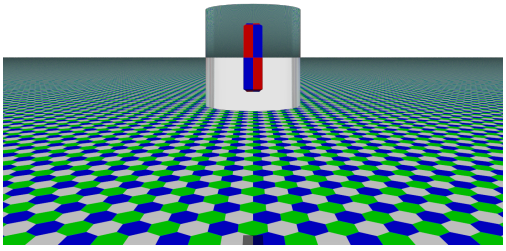

(e) Curved Slab 300 nm thick. Gradient in IOR: -2.3 to -1, through the thickness. View: X axis

Figure 15: Gradients - Curved Slabs

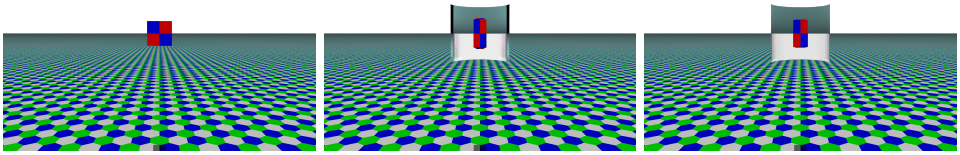

(a) Comparison cube (2 cm x 2 cm x 2 cm). View: X axis

(b) Saddle Slab 300 nm thick. Gradient in IOR: -1.1 to -0.9, through the thickness. View: X axis

(c) Saddle Slab 300 nm thick. Gradient in IOR: -2.3 to -1, through the thickness. View: X axis

Figure 16: Gradients - Saddle Slabs

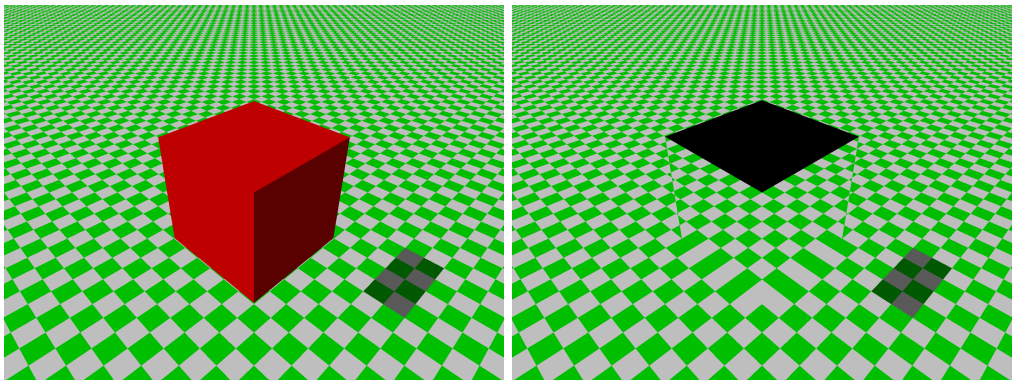

(a) Comparison cube (2 cm x 2 cm x 2 cm). View: 45°

(b) Cube cloak 300 nm thick. IOR: $\frac{1}{\sqrt{2}}$. View: 45°

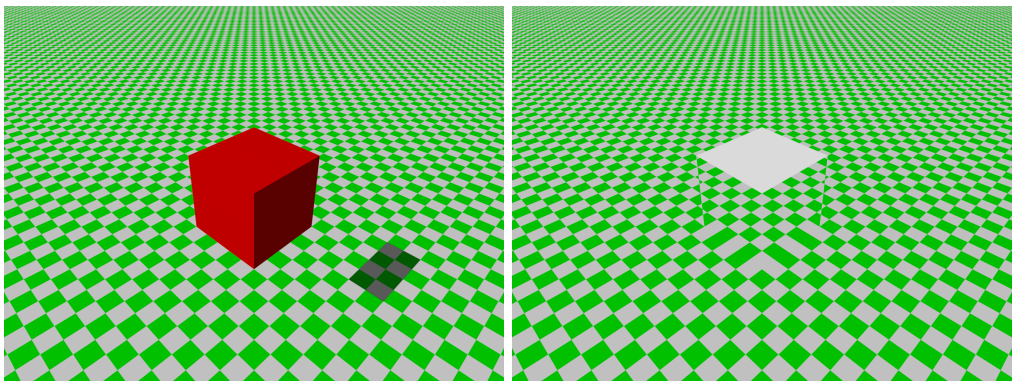

(c) Comparison cube 2 (2 cm x 2 cm x 2 cm). View: 45°

(d) Cube cloak 300 nm thick. IOR: -0.001. View: 45°

Figure 17: Embedded Objects - Cubes

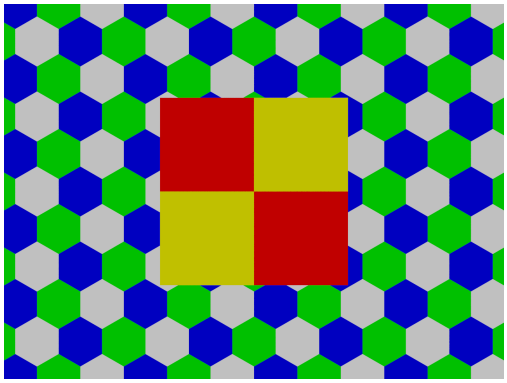

(a) Comparison cube (2 cm x 2 cm x 2 cm). View: Z axis

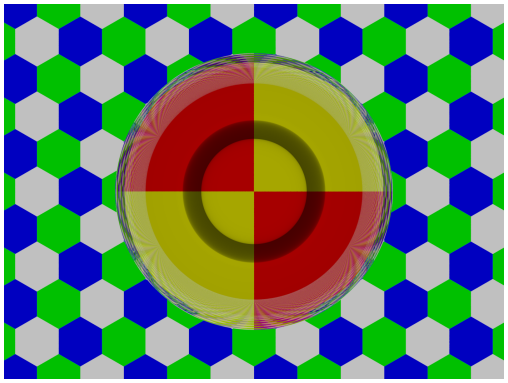

(b) Spherical cloak of radius $\sqrt{3}+0.00003$ cm. IOR: -2.3. View: Z axis

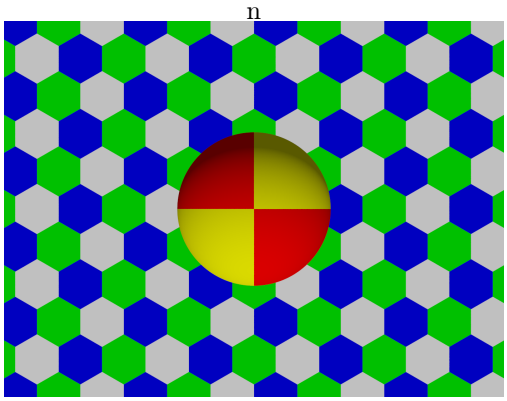

(c) Comparison sphere (radius: 1 cm). View: Z axis

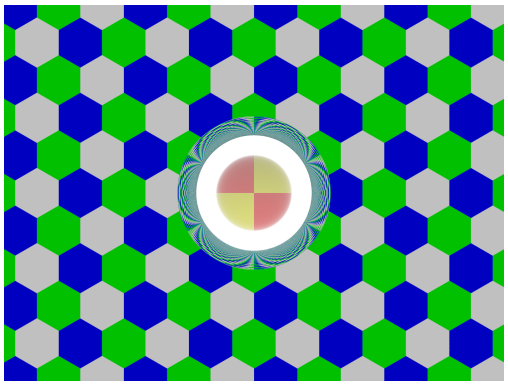

(d) Spherical cloak 300 nm thick. IOR: -0.5. View: Z axis

Figure 18: Embedded Objects - Spheres

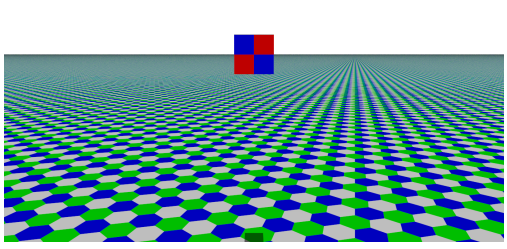

(a) Comparison cube (2 cm x 2 cm x 2 cm). View: X axis

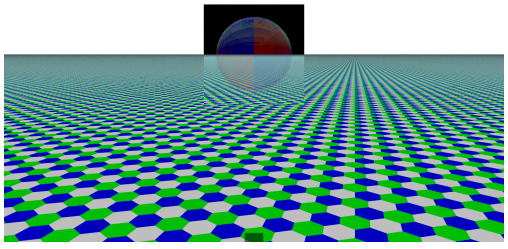

(b) Slab 5 mm thick. IOR: -0.1. View: X axis

Figure 19: Embedded Objects - Slabs

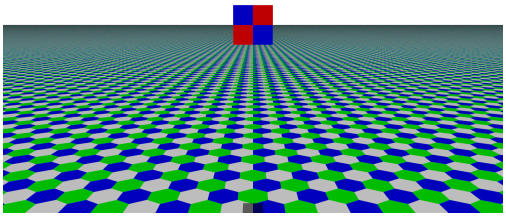

(a) Comparison cube (2 cm x 2 cm x 2 cm). View: X axis

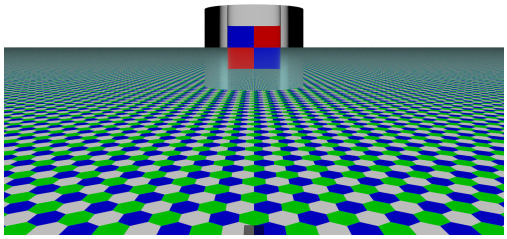

(b) Curved Slab 3 mm thick. IOR: $-\frac{1}{\sqrt{2}}$. View: X axis

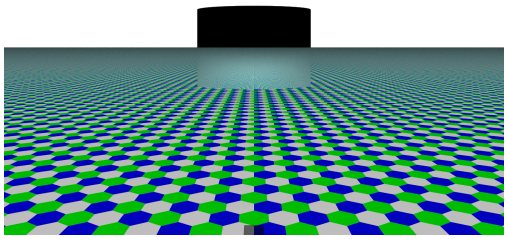

(c) Curved Slab 300 nm thick, stretched 1.5 times in the X direction. IOR: -0.01. View: X axis

Figure 20: Embedded Objects - Curved Slabs

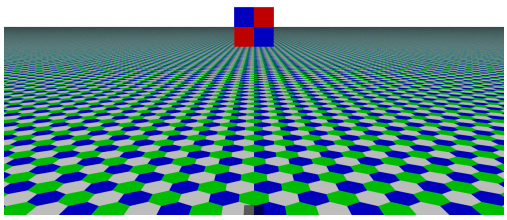

(a) Comparison cube (2 cm x 2 cm x 2 cm). View: X axis

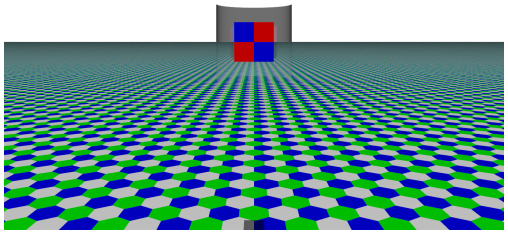

(b) Saddle Slab 300 nm thick. IOR: -2.3. View: X axis

Figure 21: Embedded Objects - Saddle Slabs

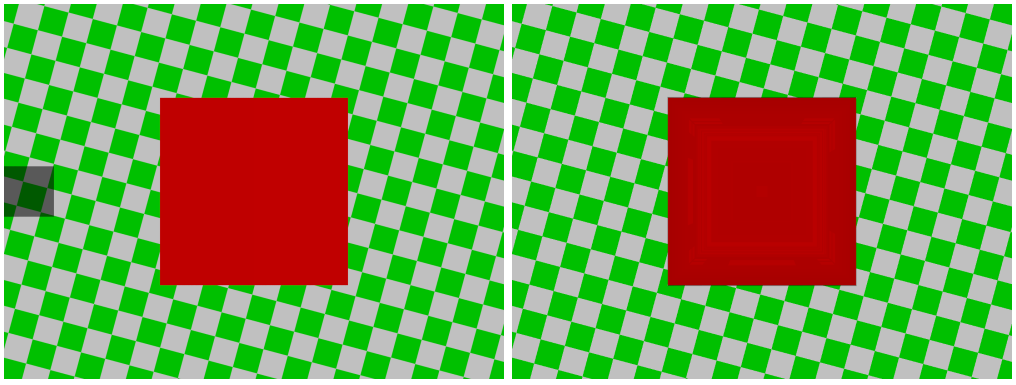

(a) Comparison cube (2 cm x 2 cm x 2 cm). View: Z axis

(b) Cube cloak 300 nm thick. Gradient in IOR: -1 to -2.3. View: Z axis

Figure 22: Surface Gradient - Cubes

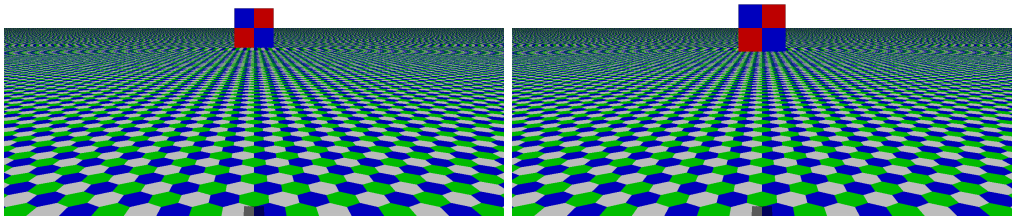

(a) Comparison cube (2 cm x 2 cm x 2 cm). View: X axis

(b) Slab 300 nm thick. Gradient in IOR: -1.1 to -0.9. View: X axis

Figure 23: Surface Gradients - Slabs

5 Challenges

5.1 Ray Tracing

At the outset of this project, little was known about the capability of POV-Ray ray tracing software to capture the effect of negative index of refraction materials for the purpose of simulating "hide-in-plain-sight" effects. For example, it was not known how to force POV-Ray to automatically calculate the reflectance and transmittance at any given point given the index of refraction. In addition, the precision which POV-Ray employed was inefficient to obtain solutions in certain cases. By adjusting the maximum transmittance value to 1, and the maximum reflectance to 1, and enforcing a requirement to conserve energy as well as to use the Fresnel Equations, POV-Ray was adequate to automatically calculate the reflectance and transmittance at any given point. However, the issues concerning precision were harder to fix. However, because POV-Ray is open source, the code was accessible, allowing changes to be made to the apropriate values, and recompiling in order to obtain the desired precision. Hence, both of these major problems have been addressed.

5.2 Finite Difference Time Domain

An elaborate technique for the estimation of the effective refractive index of a flat slab of negative index of refraction material has been presented in prior work [1], where the effective IOR calculation depends on the solution to Maxwell's equations in the coordinates of a specific feature. The solution to Maxwell's equations may be approximated via finite-difference time domain (FDTD) methods using numerical programs such as Lumerical and MEEP. In the present study, an effective refractive index is needed to conduct the ray tracing calculations using the POV-Ray software. While the technique for calculating the effective refractive index begins with a feature design in an FDTD program combined with tabular data available in the literature, a challenge exists due to the fact that POV-Ray requires a specific IOR as an input without knowing if a feature design exists that will provide the necessary IOR. A gap exists between the capability to design features in FDTD software and desired input to ray tracing software. A need exists for efficient software solutions that bridge the gap between design of NIM configurations using FDTD methods and visualization using ray tracing methods.

6 Discussion

As one can see, many different optical effects can theoretically be produced by using metamaterials. A negative index of refraction is not always required, as seen in Figures 17b and 15d. As seen in Figures 17b, 17d, and 20c, an object, here a cube, can be rendered nearly invisible. As seen in Figures 13b, 15d, 15e, 16b, 16c, 18b, 20b, and 19b, an object's apparent shape can be changed. As seen in Figures 14b, 14c, 18d, 23b, an object's apparent size can be changed. As seen in Figures 15b, 15c, 21b, an object's appearance can be multiplied to give the appearance of two or more such objects. Thus, most of the goals of this project were met.

A potential for achieving "hide-in-plain-sight" exists based upon the design of a NIM configuration combined with a morphing substructure. The results presented here indicate a variety of optical effects based upon changes in IOR and macroscopic topology of the NIM slab (i.e., flat slab, curved slab, saddle slab, etc.). It is conceived that by tailoring the object that is to be hidden to coincide with the optical effects achieved that a drastic effect on the viewer's ability to perceive the object may be achieved, thus meeting the goal of hiding the robotic platform in plain sight. Other unanticipated effects, such as dislocating shadows cast by an object, may also be exploited to achieve the goal of tricking the observer into not being able to see the object directly.

7 Conclusion and Further Research

In conclusion, the goals of this project were to investigate the use of metamaterials in hiding or disguising a micro-robotic vehicle. Several optical illusions were targeted: change in apparent shape, change in apparent size, partial or full invisibility, duplication, and translocation. Most were achieved: change in apparent shape, change in apparent size, duplication, and partial invisibility. However, these results, demonstrated by ray tracing results, using POV-Ray software, must be validated. In order to do so efficiently, a new type of software must be created - one that bridges the gap between Finite Difference Time Domain methods and Ray Tracing methods. Currently, these two types of software exist, but there is no efficient way to directly connect the nanostructure effects investigated using an FDTD software tool to the visualization response at the structural (macroscopic) level as embodied in the ray tracing results. As such, there has been an effort to validate these results using conventional FDTD techniques, but all signs indicate that the quickest way forward would be to integrate the two methods.

8 Acknowledgments

I would like to thank the following people and organizations:

- **Dr. Jaret Riddick** for taking the time and effort to mentor me throughout the summer.
- **The U.S. Army Research Lab** for providing me with this excellent opportunity.
- **Dr. Harry Atwater** for acting as Co-Mentor.
- **George Washington University** for providing financial support.

Appendices

Appendix A Proof of the Fresnel Equations

A.1 TE

$$
\begin{aligned}
E_i + E_r &= E_t \\
\frac{B_i}{\mu_i}\cos\theta_i - \frac{B_r}{\mu_r}\cos\theta_r &= \frac{B_t}{\mu_t}\cos\theta_t \\
\theta_i &= \theta_r \\
\mu_i &= \mu_r \\
B &= \frac{E}{v} \\
n &= \frac{1}{v} \\
\frac{n_i}{\mu_i}\left(E_i - E_r\right)\cos\theta_i &= \frac{n_t}{\mu_t}E_t\cos\theta_t \\
&= \frac{n_t}{\mu_t}\left(E_i + E_r\right)\cos\theta_t \\
E_i\left(\frac{n_i}{\mu_i}\cos\theta_i - \frac{n_t}{\mu_t}\cos\theta_t\right) &= E_r\left(\frac{n_i}{\mu_i}\cos\theta_i + \frac{n_t}{\mu_t}\cos\theta_t\right)
\end{aligned}
$$

$$
\begin{aligned}
\frac{E_r}{E_i} &= \frac{\frac{n_i}{\mu_i}\cos\theta_i - \frac{n_t}{\mu_t}\cos\theta_t}{\frac{n_i}{\mu_i}\cos\theta_i + \frac{n_t}{\mu_t}\cos\theta_t} \\
n &= \frac{n_t}{n_i} \\
\mu &= \frac{\mu_t}{\mu_i} \\
\frac{E_r}{E_i} &= \frac{\mu\cos\theta_i - n\cos\theta_t}{\mu\cos\theta_i + n\cos\theta_t} \\
\frac{E_t}{E_i} &= \frac{E_i + E_r}{E_i} \\
&= 1 + \frac{E_r}{E_i} \\
&= \frac{2\mu\cos\theta_i}{\mu\cos\theta_i + n\cos\theta_t} \\
R_\perp &= \left(\frac{E_r}{E_i}\right)^2 \\
&= \left(\frac{\mu\cos\theta_i - n\cos\theta_t}{\mu\cos\theta_i + n\cos\theta_t}\right)^2 \\
T_\perp &= \frac{I_t\cos\theta_t}{I_i\cos\theta_i} \\
\frac{I_t}{I_i} &= \frac{v_t\varepsilon_t E_t^2}{v_i\varepsilon_i E_i^2} \\
&= \frac{\mu_i\mu_t v_t\varepsilon_t}{\mu_t\mu_i v_i\varepsilon_i}t^2 \\
\frac{c}{v_t} &= c\sqrt{\mu_t\varepsilon_t} \\
\sqrt{\mu_t\varepsilon_t} &= \frac{1}{v_t} \\
&= \frac{n_t}{c} \\
\mu_t\varepsilon_t &= \frac{1}{v_t^2} \\
&= \frac{n_t^2}{c^2} \\
v_t\mu_t\varepsilon_t &= \frac{1}{v_t} \\
&= \frac{n_t^2 v_t}{c^2} \\
n_t &= \frac{c}{v_t} \\
v_t\mu_t\varepsilon_t &= \frac{n_t}{c} \\
\frac{I_t}{I_i} &= \frac{\mu_i n_t}{\mu_t n_i}t^2 \\
T_\perp &= \frac{n}{\mu}\left(\frac{\cos\theta_t}{\cos\theta_i}\right)\left(\frac{2\mu\cos\theta_i}{\mu\cos\theta_i + n\cos\theta_t}\right)^2
\end{aligned}
$$

A.2 TM

$$
\begin{aligned}
E_i \cos\theta_i - E_r \cos\theta_r &= E_t \cos\theta_t \\
\frac{n_i}{\mu_i}(E_i + E_r) &= \frac{n_t}{\mu_t} E_t \\
\theta_i &= \theta_r \\
\frac{n_t}{\mu_t}(E_i - E_r)\cos\theta_i &= \frac{n_t}{\mu_t} E_t \cos\theta_t \\
&= \frac{n_i}{\mu_i}(E_i + E_r)\cos\theta_t \\
E_i\left(\frac{n_t}{\mu_t}\cos\theta_i - \frac{n_i}{\mu_i}\cos\theta_t\right) &= E_r\left(\frac{n_t}{\mu_t}\cos\theta_i + \frac{n_i}{\mu_i}\cos\theta_t\right) \\
\frac{E_r}{E_i} &= \frac{\frac{n_t}{\mu_t}\cos\theta_i - \frac{n_i}{\mu_i}\cos\theta_t}{\frac{n_t}{\mu_t}\cos\theta_i + \frac{n_i}{\mu_i}\cos\theta_t} \\
n &= \frac{n_t}{n_i} \\
\mu &= \frac{\mu_t}{\mu_i} \\
\frac{E_r}{E_i} &= \frac{n\cos\theta_i - \mu\cos\theta_t}{n\cos\theta_i + \mu\cos\theta_t} \\
\frac{E_t}{E_i} &= \frac{\mu}{n}\left(1 + \frac{E_r}{E_i}\right) \\
&= \frac{\mu}{n}\left(\frac{2n\cos\theta_i}{n\cos\theta_i + \mu\cos\theta_t}\right) \\
&= \frac{2\mu\cos\theta_i}{n\cos\theta_i + \mu\cos\theta_t} \\
R_\parallel &= \left(\frac{n\cos\theta_i - \mu\cos\theta_t}{n\cos\theta_i + \mu\cos\theta_t}\right)^2 \\
T_\parallel &= \frac{n}{\mu}\left(\frac{\cos\theta_t}{\cos\theta_i}\right)\left(\frac{2\mu\cos\theta_i}{n\cos\theta_i + \mu\cos\theta_t}\right)^2
\end{aligned}
$$

References

[1] Stanley P. Burgos, Rene deWaele, Albert Polman, and Harry A. Atwater. A single-layer wide-angle negative-index metamaterial at visible frequencies. *Nature Materials*, 9(5):407–412, May 2010. URL `http://dx.doi.org/10.1038/nmat2747`.

[2] M.-K. Dano and M.W. Hyer. Sma-induced snap-through of unsymmetric fiber-reinforced composite laminates. *International Journal of Solids and Structures*, 40:5949–5972, 2003.

[3] Gunnar Dolling, Martin Wegener, Stefan Linden, and Christoph Hormann. Photorealistic images of objects in effective negative-index materials. *Optics Express*, 14(5):1842–1849, March 2006.

[4] C. García-Meca, R. Ortuño, F.J. Rodríguez-Fortuño, A. Martínez, and J. Martí. Extraordinary optical transmission with negative index of refraction. *Metamaterials*, pages 515–517, September 2008.

[5] Eugene Hecht. *Optics*. Pearson Education, 4 edition, 2002.

[6] Yosuke Minowa, Takashi Fujii, Masaya Nagai, Tetsuyuki Ochiai, Kazuaki Sakoda, Kazuyuki Hirao, and Koichiro Tanaka. Evaluation of effective electric permittivity and magnetic permeability in metamaterial slabs by terahertz time-domain spectroscopy. *Optics Express*, 16(7):4785 – 4796, March 2008.

[7] Peter J. Mohr, Barry N. Taylor, and David B. Newell. CODATA recommended values of the fundamental physicsal constants: 2006. *Reviews of Modern Physics*, 80:633–730, June 2008. doi: 10.1103/RevModPhys.80.633. URL `http://link.aps.org/doi/10.1103/RevModPhys.80.633`.

[8] L. Novotny and C. Hafner. Light propogation in a cylindrical waveguide with a complex, metallic, dielectric function. *Physical Review E*, 50(5):4094–4106, November 1994.

[9] John Pendry. All smoke and metamaterials. *Nature*, 460(30):579–580, July 2009.

[10] Vladimir M. Shalaev, Wenshan Cai, Uday K. Chettiar, Hsiao-Kuan Yuan, Andrey K. Sarychev, Vladimir P. Drachev, and Alexander V. Kildishev. Negative index of refraction in optical metamaterials. *Optics Letters*, 30(24):3356–3358, December 2005.

[11] D. R. Smith, D. C. Vier, Th. Koschny, and C. M. Soukoulis. Electromagnetic parameter retrieval from inhomogeneous metamaterials. *Physical Review E*, 71:036617, March 2005.

[12] V.G. Veselago. The electrodynamics of substances with simultaneously negative values of ε and μ. *Soviet Physics Uspekhi*, 10:509–514, 1968. URL `http://stacks.iop.org/0038-5670/10/i=4/a=R04`.